ULTRACOLD CHEMISTRY

Resonant collisional shielding of reactive molecules using electric fields

Kyle Matsuda[1]*, Luigi De Marco[1], Jun-Ru Li[1], William G. Tobias[1], Giacomo Valtolina[1], Goulven Quéméner[2], Jun Ye[1]*

Full control of molecular interactions, including reactive losses, would open new frontiers in quantum science. We demonstrate extreme tunability of ultracold chemical reaction rates by inducing resonant dipolar interactions by means of an external electric field. We prepared fermionic potassium-rubidium molecules in their first excited rotational state and observed a modulation of the chemical reaction rate by three orders of magnitude as we tuned the electric field strength by a few percent across resonance. In a quasi–two-dimensional geometry, we accurately determined the contributions from the three dominant angular momentum projections of the collisions. Using the resonant features, we shielded the molecules from loss and suppressed the reaction rate by an order of magnitude below the background value, thereby realizing a long-lived sample of polar molecules in large electric fields.

Controlling chemical reactions and collisions has been a central focus of work on cold and ultracold molecules (*1*–*6*). Progress in cooling and trapping molecules has led to exciting advances in this area, including the precise characterization of scattering resonances (*7*–*9*), the observation of atom-molecule (*10*) and molecule-molecule (*11*–*13*) cold collisions, and the synthesis of new chemical species (*14*). In particular, ultracold polar molecules, for which both internal and external degrees of freedom are controlled, present distinctive opportunities (*15*–*26*). At ultralow temperatures, small perturbations to the long-range intermolecular potential, although negligible relative to chemical bonding energy scales, can vastly exceed the kinetic energy of the colliding molecules and thus strongly alter the rate of chemical reactions at close range (*3*). This sensitivity, combined with the rich structure of polar molecules and their tunability using external electromagnetic fields, suggests the exciting possibility of precisely controlling reactions (*1*, *4*–*6*). In addition to providing insights about fundamental chemical processes (*27*, *28*), such control would aid in the production of quantum-degenerate molecular gases (*29*–*31*) and could facilitate precision measurements (*32*) or studies of many-body physics (*33*) in these systems.

Applying an electric field $\mathbf{E}$ strongly modifies the reaction rates of ultracold polar molecules via dipolar interactions (*34*, *35*). In the ultracold regime, molecules collide predominantly in the lowest partial wave L allowed by quantum statistics ($L = 1$ for identical fermions). Owing to the anisotropy of the dipolar interaction, the likelihood of two molecules meeting at short range depends on how they approach each other relative to the direction of the induced dipole, or more formally, on the projection m_L of L onto the axis of $\mathbf{E}$. For fermionic molecules in three dimensions (3D), attractive head-to-tail ($m_L = 0$) collisions lead to rapid losses (*34*), which scale as d^6 in the induced dipole moment d (*36*). If the molecules are instead trapped in a quasi–two-dimensional (quasi-2D) geometry with $\mathbf{E}$ along the strongly confined direction, only repulsive side-to-side ($m_L = \pm 1$) collisions are allowed, suppressing losses and enhancing the elastic collision rate (*37*, *38*). For ground-state potassium-rubidium (KRb) molecules, we recently used this approach to achieve a ratio of elastic collisions to reactive collisions exceeding 100 (*31*).

Here, we experimentally demonstrate a striking effect of the electric field on molecular collisions: Chemical reaction rates in an ultracold gas of molecules are sharply varied by three orders of magnitude near particular values of the field strength $|\mathbf{E}|$. These values occur where higher rotationally excited states become degenerate with the initial collision channel, inducing resonant dipolar interactions that profoundly alter the long-range potential and hence the reaction rate (*39*). Although losses can also be resonantly enhanced, the most important effect is the substantial suppression of loss for an appropriate choice of $|\mathbf{E}|$. This shielding mechanism was first proposed by Avdeenkov *et al.* (*40*), and related theory was subsequently extended to a wide variety of bosonic and fermionic species of experimental interest (*39*, *41*, *42*). Alternatively, the use of microwave (*43*–*47*) or optical (*48*) dressing to suppress molecular loss has been proposed. However, microwave dressing has so far only led to an enhanced loss rate in experiments (*49*, *50*).

We prepared ultracold fermionic $^{40}K^{87}Rb$ molecules in the $|N, m_N\rangle = |1,0\rangle$ state, where N is the rotational angular momentum and m_N is its projection onto the axis of $\mathbf{E}$. Throughout, $|N, m_N\rangle|N', m'_N\rangle$ denotes the combined molecular state of a pair of molecules with one molecule in $|N, m_N\rangle$ and the other in $|N', m'_N\rangle$. We observed a drastic change in the two-body reactive loss rate near two field strengths, $|\mathbf{E}_1| = 11.72$ kV/cm and $|\mathbf{E}_2| = 12.51$ kV/cm, where the energies of $|0,0\rangle|2,\pm1\rangle$ and $|0,0\rangle|2,0\rangle$ (respectively) cross the energy of $|1,0\rangle|1,0\rangle$ (Fig. 1A). Near these crossings (Fig. 1B), the nearly degenerate states are resonantly coupled by dipolar interactions, becoming strongly mixed as the molecules approach to separations $r \sim r_0$ during a collision event, where $r_0 = 270a_0$ is the radius of the p-wave centrifugal barrier (*51*) and a_0 is the Bohr radius.

The consequence of this r-dependent state mixing is apparent in the adiabatic energy curves near $|\mathbf{E}_2|$ (Fig. 1C) (*52*). For $|\mathbf{E}| > |\mathbf{E}_2|$ (orange line), the energy of $|1,0\rangle|1,0\rangle$ is higher than that of $|0,0\rangle|2,0\rangle$. Hence, coupling between the states causes an increasing energy of $|1,0\rangle$ molecules as they approach, creating a repulsive barrier (with height ~ 300 μK) that is three orders of magnitude larger than the typical collision energy set by the temperature of the gas (250 nK). In this case, molecules are shielded from reactive losses, because they cannot meet at short range except by tunneling through the barrier (which occurs with a low probability). Conversely, for $|\mathbf{E}| < |\mathbf{E}_2|$ (green line), the energy of $|1,0\rangle|1,0\rangle$ is lower than that of $|0,0\rangle|2,0\rangle$, resulting in an attractive interaction and an enhanced loss rate. For comparison, the diabatic energy curve (black line) shows the behavior in the absence of resonant dipolar interactions. Although lossy collisions are suppressed for $|\mathbf{E}|$ just above resonance, elastic dipolar collisions for KRb are predicted to be nearly unaffected by the shielding (*39*). In general, the shielding is predicted to increase the ratio of elastic collisions to reactive collisions, potentially allowing for efficient evaporative cooling of molecules in 3D (*42*) and complementing the recently demonstrated evaporation in 2D (*31*).

This effect is akin to a Förster resonance—for example, between Rydberg atoms (*53*–*55*), in which $|\mathbf{E}|$ is tuned to create degeneracies between pairs of dipole-coupled states, resulting in resonant energy transfer. A key difference is the much smaller dipole moment of molecules relative to that of Rydberg atoms. Consequently, colliding molecules experience an adiabatic increase in the dipolar interaction energy as they approach. We stress that this is not a conventional scattering resonance arising from the presence of a molecule-molecule

[1]JILA, National Institute of Standards and Technology, and Department of Physics, University of Colorado, Boulder, CO 80309, USA. [2]Université Paris-Saclay, CNRS, Laboratoire Aimé Cotton, 91405 Orsay, France.
*Corresponding author. Email: kyle.matsuda@colorado.edu (K.M.); ye@jila.colorado.edu (J.Y.)

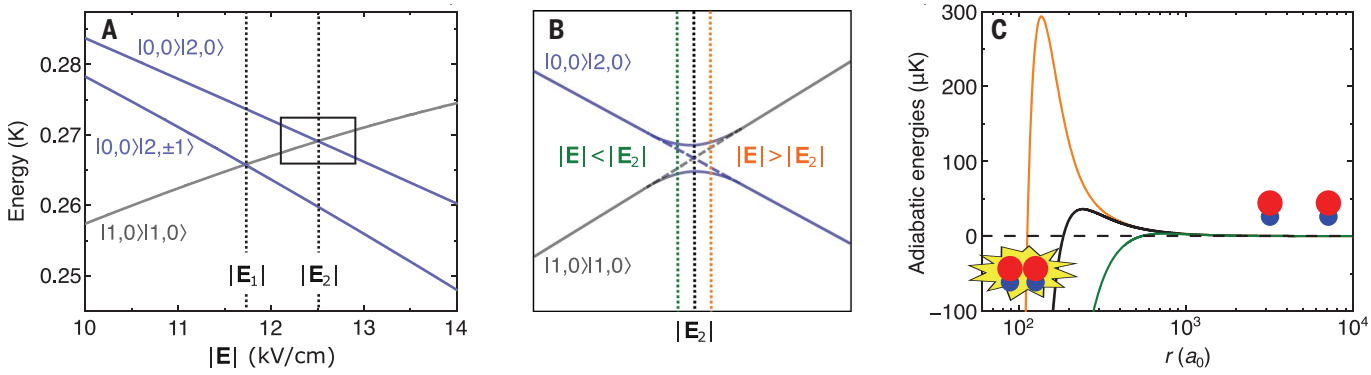

Fig. 1. Electric field–induced shielding. (**A**) Energies of the relevant combined molecular states as a function of $|\mathbf{E}|$, displaying the crossing of $|1,0\rangle|1,0\rangle$ with $|0,0\rangle|2,\pm1\rangle$ and $|0,0\rangle|2,0\rangle$. (**B**) Qualitative picture of the region near $|\mathbf{E}_2|$ (black dotted line). For large molecular separations $r >> r_0$ (dashed lines), the two states are not coupled. For separations $r \sim r_0$ (solid lines), an avoided crossing is opened as a result of dipolar interactions between the states. As two $|1,0\rangle$ molecules collide at a fixed $|\mathbf{E}| > |\mathbf{E}_2|$ (orange dotted line), the avoided crossing results in an effective repulsion; at a fixed $|\mathbf{E}| < |\mathbf{E}_2|$ (green dotted line), the avoided crossing results in an effective attraction. The same argument applies near $|\mathbf{E}_1|$. (**C**) Adiabatic energy curves for KRb molecules in $|1,0\rangle$ colliding with $m_L = \pm1$ at $|\mathbf{E}| = 12.504$ kV/cm (green curve) and 12.670 kV/cm (orange curve), corresponding to the values of $|\mathbf{E}|$ indicated by the green and orange vertical dotted lines in (B). The diabatic energy curve at 12.670 kV/cm (black solid curve) shows a barrier (36 μK) from the sum of the centrifugal (24 μK) barrier (*51*) and the semiclassical dipolar (12 μK) barrier (*31*, *37*, *38*) in the absence of resonant dipolar interactions. The dashed line shows the average collision energy of 250 nK. The red and blue spheres represent Rb and K, respectively.

bound state, but rather a resonance between two free scattering states enabled by the internal structure of the molecules (*39*).

The experimental setup has been described in detail previously (*31*). In brief, a degenerate mixture of ^{40}K and ^{87}Rb was prepared in six layers of a 1D optical lattice, with final trap frequencies $(\omega_x, \omega_y, \omega_z) = 2\pi \times (34, 17.7 \times 10^3, 34)$ Hz for KRb in each layer (gravity points along $-\hat{y}$). Weakly bound molecules were created with a magnetic field ramp through an interspecies Feshbach resonance at 546.62 G and were transferred to the ro-vibronic ground state by stimulated Raman adiabatic passage (STIRAP) at $|\mathbf{E}_{\mathrm{STIRAP}}| = 4.5$ kV/cm with the field along $+\hat{y}$. For studying the $|1,0\rangle$ state, it was advantageous to perform STIRAP at large $|\mathbf{E}|$ to bypass several avoided crossings at $|\mathbf{E}| <$ 1 kV/cm that arise from the hyperfine structure (*21*). Typical starting conditions were 2×10^4 molecules in the $|0,0\rangle$ state at a temperature $T = 250$ nK, corresponding to about 1.8 times the Fermi temperature. With nearly perfect occupancy of the lowest band ($k_B T/\hbar\omega_y \sim 0.3$, where k_B is the Boltzmann constant and $\hbar$ is the reduced Planck constant) and negligible tunneling between lattice sites, our system realized a stack of quasi-2D molecular gases.

To measure the reactive loss of the $|1,0\rangle$ state, we used the following protocol. Starting at $\mathbf{E}_{\mathrm{STIRAP}}$, we first applied a microwave π-pulse to transfer the molecules from $|0,0\rangle$ to $|1,0\rangle$ with a Rabi frequency of $2\pi \times 200$ kHz and a typical efficiency above 95%. Any remaining $|0,0\rangle$ population was quickly lost in a few milliseconds via *s*-wave reactive collisions with $|1,0\rangle$. Next, $\mathbf{E}$ was ramped to its target configuration in 60 ms. After a variable hold time t, $\mathbf{E}$ was ramped back to $\mathbf{E}_{\mathrm{STIRAP}}$ in 60 ms. To image $|1,0\rangle$ molecules, we applied another microwave pulse to transfer the molecules back to the $|0,0\rangle$ state, then used STIRAP to transfer to the Feshbach state before imaging the molecules in time-of-flight expansion. A constant magnetic field of 545.5 G was present during the measurements. We fitted the measured average density n as a function of t to the solution of the two-body loss rate equation $dn/dt = -\beta n^2$, where β is the two-body chemical reaction rate coefficient. In 2D, there is no temperature increase associated with the two-body loss (*31*, *56*), hence this rate equation is simplified in comparison to 3D (*29*).

To fully characterize the shielding effect, we first show how to tune the angular momentum character of the collisions by changing the orientation of $\mathbf{E}$ relative to the quasi-2D planes.

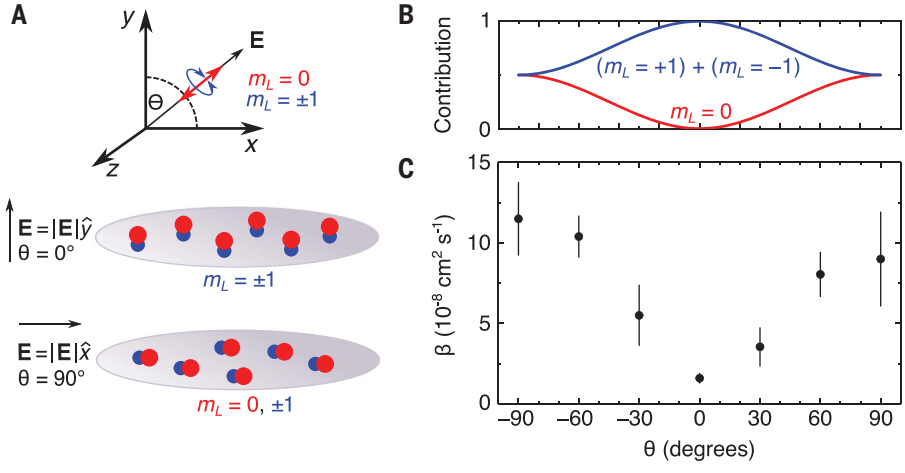

Fig. 2. Experimental setup and control of reactions by the electric field orientation. (**A**) Schematic of the experiment geometry. Owing to the strong confinement along $\hat{y}$, the m_L states participating in the collisions can be controlled with θ. (**B**) Contribution of the $m_L = 0$ (red) or $m_L = \pm1$ (blue) channels to the scattering as a function of θ. (**C**) β as a function of θ for a fixed bias strength $|\mathbf{E}| = 7.09$ kV/cm. Error bars are 1 SE from fits to the two-body rate equation.

Previous measurements in quasi-2D with $\mathbf{E}$ oriented along the tightly confined direction ($\hat{y}$) showed a suppression of β at moderately large values of d owing to repulsive $m_L = \pm1$ dipolar collisions (*31*, *37*). Here, we studied the dipolar anisotropy by tilting $\mathbf{E}$ away from the y axis by an angle θ, which enabled controlled mixing of the attractive $m_L = 0$ collisions into the scattering (Fig. 2A). Although the dipolar interaction in general mixes higher partial waves into the scattering, contributions from $|m_L| > 1$ are negligible for the relatively small values of d explored here (*52*).

Although the collisions always occurred along the $\hat{x}$ and $\hat{z}$ directions because of the strong confinement along $\hat{y}$, the angular momentum

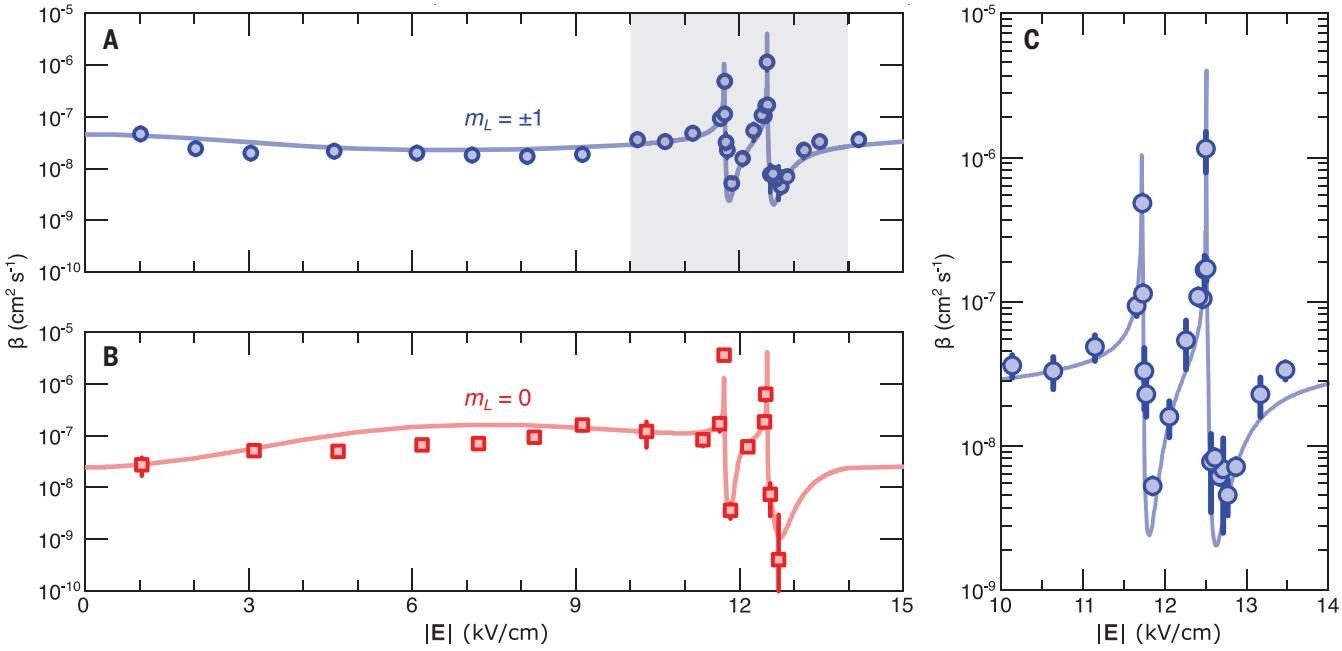

Fig. 3. 3D characterization of the shielding effect. (**A**) $\beta_{\pm1}$ (blue circles) versus |**E**| extracted from loss measurements at θ = 0°. (**B**) β_0 (red squares) versus |**E**| extracted from loss measurements at θ = 90° and 0°. In (A) and (B), solid lines are theoretical predictions for the experimental T = 250 nK and $\omega_y = 2\pi \times 17.7$ kHz with no free parameters. Error bars are 1 SE from fits to the two-body rate equation. (**C**) Close-up of $\beta_{\pm1}$ in the region near $|\mathbf{E}_1|$ and $|\mathbf{E}_2|$ [gray shaded region of (A)].

character of the collisions with respect to **E** changed with θ. For θ = 0°, the collisions decomposed equally into the m_L = ±1 channels, which give equal contributions to the collision cross section as a result of the azimuthal symmetry of the dipolar interaction. For θ = 90°, collisions along $\hat{x}$ corresponded to m_L = 0 scattering, and those along $\hat{z}$ were still an equal superposition of the m_L = ±1 channels. Hence, by measuring β at θ = 0° and 90°, it was possible to extract the loss rate coefficients $\beta_{\pm1}$ and β_0 associated with the m_L = ±1 and 0 channels, respectively. The full dependence on θ (Fig. 2B) was calculated by considering the mixing of the m_L states under rotations (*52*).

Figure 2C shows the measured β for |1,0⟩ molecules at |**E**| = 7.09 kV/cm as θ was varied over 180°. As expected, β increased with |θ| and reached a maximum at θ = ± 90°, where attractive m_L = 0 collisions dominated the loss rate. At 7.09 kV/cm, the relatively small value of d = −0.12 D limited the maximum increase of β to only an order of magnitude, in contrast to the much larger effect expected for larger |d| (*57*). Our electrode geometry permitted excellent control of the curvature of **E** along $\hat{x}$, except near θ = ± 90° (fig. S1), where we applied a small correction to the measured β to account for compression of the cloud attributable to the increased curvature in this configuration (*52*).

Having controlled the angular momentum channels participating in the collisions, we proceeded to explore the dependence of the |1,0⟩ reaction rate on **E**. We measured β at both θ = 0° and 90° to extract $\beta_{\pm1}$ and β_0 as a function of |**E**| (*52*), as summarized in Fig. 3, A and B, respectively. For both values of θ, we calibrated |**E**| to a few parts in 10^4 using spectroscopy on the |0,0⟩ to |1,0⟩ transition.

In the background region (|**E**| = 1 to 11 kV/cm) away from resonance, we observed a slight decrease in $\beta_{\pm1}$ and a corresponding increase in β_0. $\beta_{\pm1}$ reached a minimum and β_0 reached a maximum near |**E**| = 7 kV/cm, in agreement with theoretical predictions (Fig. 3, A and B, solid lines) (*52*). To understand the trends of $\beta_{\pm1}$ and β_0, we note that |d| is nonmonotonic in the investigated range of |**E**| and reaches a maximum of 0.12 D at 7 kV/cm. Thus, the trends of $\beta_{\pm1}$ and β_0 are consistent with the semiclassical picture of repulsive side-to-side (m_L = ±1) or attractive head-to-tail (m_L = 0) dipolar collisions modifying the loss rate, as previously measured for the N = 0 state (*31*, *37*, *38*). Away from resonance, our results illustrate the universal nature of this semiclassical effect, depending only on the value of |d| and not on the rotational state of the molecule, when resonant dipolar effects are not important. In addition, the absence of any field-dependent Fano-Feshbach resonances is consistent with universal (unit probability) loss at short range for the |1,0⟩ state (*51*), as previously measured with N = 0 molecules (*34*, *35*).

In the region near $|\mathbf{E}_1|$ and $|\mathbf{E}_2|$, resonant off-diagonal dipolar couplings to |0,0⟩|2,±1⟩ and |0,0⟩|2,0⟩ become the dominant contribution, instead of the diagonal dipolar interactions that determine β in the background region. Here, inelastic collisions, which result in transitions to the nearby combined molecular state, are possible owing to the long-range dipolar mixing of the states. Because only |1,0⟩ molecules were detected in the experiment, the measured loss rate consisted of the sum of the inelastic and reactive rates, with the inelastic rate predicted to be negligible except for within a small range of |**E**| near resonance (*39*). The optimal shielding condition, where the overall loss is minimized, arises from a competition between the changes in the height of the repulsive barrier and the inelastic loss rate, with the inelastic rate falling off faster away from resonance (*39*).

We observed sharp features at $|\mathbf{E}_1|$ and $|\mathbf{E}_2|$ in both the m_L = ±1 and m_L = 0 channels, in excellent quantitative agreement with the scattering theory predictions with no free parameters (Fig. 3, A and B, solid lines) (*52*). We measured a maximum variation of $\beta_{\pm1}$ by a factor of 300 ± 20, and a reduction in $\beta_{\pm1}$ by a factor of 8 ± 3 at the optimal shielding condition (12.77 kV/cm) relative to the value away from the features (10.13 kV/cm). In the m_L = 0 channel, we observed a variation of β_0 by a factor of 1000 ± 400 near the features. Comparing the measurements at the optimal shielding point (11.84 kV/cm) and away from the features (11.32 kV/cm), we observed a maximum suppression of β_0 by a factor of 23 ± 10 below its background value. (We excluded the point at 12.72 kV/cm from this analysis, because the extracted β_0 was consistent with zero within our measurement precision.)

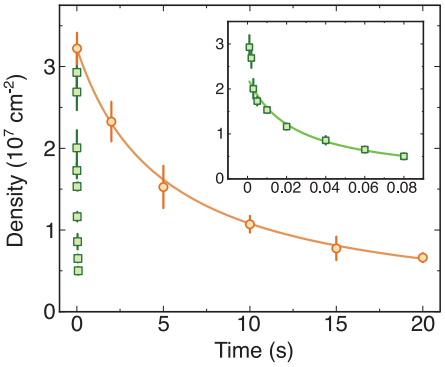

Fig. 4. Reaction shielding and enhancement near $|\mathbf{E}_2|$. Molecular loss measurements at $|\mathbf{E}|$ = 12.50 kV/cm (green squares) and 12.67 kV/cm (orange circles) for $\theta = 0°$ are shown. The inset shows the data for $|\mathbf{E}|$ = 12.50 kV/cm on an enlarged *x* axis. Solid lines are fits to the two-body rate equation; error bars are 1 SE of independent measurements.

As opposed to the semiclassical nature of the loss suppression when dipolar molecules are made to collide side-to-side (*31*, *37*), the presence of the resonances in both the $m_L = 0$ and $m_L = \pm 1$ channels highlights the quantum nature of the shielding mechanism, which is based on level repulsion between the two combined molecular states brought to degeneracy by **E**. The effect occurs independently of the relative orientation of the dipoles, because approaching with either $m_L = 0$ or $m_L = \pm 1$ causes dipolar mixing of the states. Our quasi-2D measurements indicated that the shielding is present in all three of these channels at the same values of $|\mathbf{E}|$, even in the case of $m_L = 0$ where the dipoles approach in attractive head-to-tail collisions. We thus fully expect that the shielding will also be effective in 3D (*39*).

Figure 3C shows a close-up of $\beta_{\pm 1}$ near $|\mathbf{E}_1|$ and $|\mathbf{E}_2|$, emphasizing the narrow widths of the features. An intuitive explanation for the observed widths, which were on the order of tens of V/cm, comes from comparing the resonant dipolar interaction energy with the Stark shift of the two crossing states. Away from resonance, the reaction rate is controlled by the height of the *p*-wave centrifugal barrier, which occurs at r_0 (*51*). Near resonance, this barrier is modified by the dipolar coupling V_{dd} between the states, with an approximate energy scale of $V_{dd} \sim d_0^2/4\pi\varepsilon_0 r_0^3 = h \times (16\,\mathrm{MHz})$, where $d_0 = 0.574$ D is the permanent dipole moment, ε_0 is the permittivity of free space, and h is the Planck constant. The differential Stark shift of $|1,0\rangle|1,0\rangle$ and $|0,0\rangle|2,0\rangle$ near 12 kV/cm is roughly $\partial U/\partial|\mathbf{E}| = h \times 215$ kHz/(V/cm). This argument suggests a width on the order of $V_{dd}/(\partial U/\partial|\mathbf{E}|) = 75$ V/cm, in qualitative agreement with the exact result from scattering calculations.

To underscore the enormous change in β under a small variation of $|\mathbf{E}|$, Fig. 4 displays two molecular loss curves in the vicinity of $|\mathbf{E}_2|$ at $\theta = 0°$, corresponding to the largest measured difference in $\beta_{\pm 1}$. The values of $|\mathbf{E}|$ for the two curves, 12.50 kV/cm (green squares and inset) and 12.67 kV/cm (orange circles), correspond to the adiabatic energy curves in Fig. 1C. At $|\mathbf{E}| = 12.50$ kV/cm, the loss rate was strongly enhanced and the molecules were lost within 100 ms. In contrast, at $|\mathbf{E}| = 12.67$ kV/cm, the molecules were shielded from loss and ~20% of the initial density was still detected after 20 s of hold time, thereby realizing a long-lived gas of polar molecules in a large electric field.

We have demonstrated a method for controlling reactive losses using an external electric field and find excellent agreement with theoretical predictions. Our investigation of the $m_L = 0$ and $m_L = \pm 1$ collision channels strongly suggests that the shielding remains effective in 3D geometry, without the need for an optical lattice to protect the molecules. Indeed, we have made preliminary observations of long-lived molecules in a crossed optical dipole trap at 12.67 kV/cm. The shielding could be used to create a favorable ratio of elastic to reactive collisions for evaporative cooling, which would simplify future efforts to create quantum-degenerate molecular gases for species other than KRb (*41*, *42*). These results provide long-lived quantum gases of polar molecules in strong electric fields that are ready to be used to explore a wide range of exciting many-body phenomena and quantum information applications.

REFERENCES AND NOTES

1. R. V. Krems, *Phys. Chem. Chem. Phys.* **10**, 4079–4092 (2008).
2. L. D. Carr, D. DeMille, R. V. Krems, J. Ye, *New J. Phys.* **11**, 055049 (2009).
3. G. Quéméner, P. S. Julienne, *Chem. Rev.* **112**, 4949–5011 (2012).
4. M. Lemeshko, R. V. Krems, J. M. Doyle, S. Kais, *Mol. Phys.* **111**, 1648–1682 (2013).
5. N. Balakrishnan, *J. Chem. Phys.* **145**, 150901 (2016).
6. J. L. Bohn, A. M. Rey, J. Ye, *Science* **357**, 1002–1010 (2017).
7. S. Chefdeville *et al.*, *Science* **341**, 1094–1096 (2013).
8. A. Klein *et al.*, *Nat. Phys.* **13**, 35–38 (2017).
9. T. de Jongh *et al.*, *Science* **368**, 626–630 (2020).
10. M. T. Hummon *et al.*, *Phys. Rev. Lett.* **106**, 053201 (2011).
11. B. C. Sawyer *et al.*, *Phys. Chem. Chem. Phys.* **13**, 19059–19066 (2011).
12. X. Wu *et al.*, *Science* **358**, 645–648 (2017).
13. Y. Segev *et al.*, *Nature* **572**, 189–193 (2019).
14. P. Puri *et al.*, *Science* **357**, 1370–1375 (2017).
15. K. K. Ni *et al.*, *Science* **322**, 231–235 (2008).
16. T. Takekoshi *et al.*, *Phys. Rev. Lett.* **113**, 205301 (2014).
17. P. K. Molony *et al.*, *Phys. Rev. Lett.* **113**, 255301 (2014).
18. J. W. Park, S. A. Will, M. W. Zwierlein, *Phys. Rev. Lett.* **114**, 205302 (2015).
19. M. Guo *et al.*, *Phys. Rev. Lett.* **116**, 205303 (2016).
20. T. M. Rvachov *et al.*, *Phys. Rev. Lett.* **119**, 143001 (2017).
21. F. Seeßelberg *et al.*, *Phys. Rev. Lett.* **121**, 253401 (2018).
22. H. Yang *et al.*, *Science* **363**, 261–264 (2019).
23. E. S. Shuman, J. F. Barry, D. Demille, *Nature* **467**, 820–823 (2010).
24. S. Truppe *et al.*, *Nat. Phys.* **13**, 1173–1176 (2017).
25. L. W. Cheuk *et al.*, *Phys. Rev. Lett.* **125**, 043401 (2020).
26. S. Ding, Y. Wu, I. A. Finneran, J. J. Burau, J. Ye, *Phys. Rev. X* **10**, 021049 (2020).
27. S. Ospelkaus *et al.*, *Science* **327**, 853–857 (2010).
28. M. G. Hu *et al.*, *Science* **366**, 1111–1115 (2019).
29. L. De Marco *et al.*, *Science* **363**, 853–856 (2019).
30. W. G. Tobias *et al.*, *Phys. Rev. Lett.* **124**, 033401 (2020).
31. G. Valtolina *et al.*, *Nature* **588**, 239–243 (2020).
32. D. DeMille, J. M. Doyle, A. O. Sushkov, *Science* **357**, 990–994 (2017).
33. M. A. Baranov, M. Dalmonte, G. Pupillo, P. Zoller, *Chem. Rev.* **112**, 5012–5061 (2012).
34. K. K. Ni *et al.*, *Nature* **464**, 1324–1328 (2010).
35. M. Guo *et al.*, *Phys. Rev. X* **8**, 041044 (2018).
36. G. Quéméner, J. L. Bohn, *Phys. Rev. A* **81**, 022702 (2010).
37. M. H. G. de Miranda *et al.*, *Nat. Phys.* **7**, 502–507 (2011).
38. G. Quéméner, J. L. Bohn, *Phys. Rev. A* **83**, 012705 (2011).
39. G. Wang, G. Quéméner, *New J. Phys.* **17**, 035015 (2015).
40. A. V. Avdeenkov, M. Kajita, J. L. Bohn, *Phys. Rev. A* **73**, 022707 (2006).
41. G. Quéméner, J. L. Bohn, *Phys. Rev. A* **93**, 012704 (2016).
42. M. L. González-Martínez, J. L. Bohn, G. Quéméner, *Phys. Rev. A* **96**, 032718 (2017).
43. H. P. Büchler *et al.*, *Phys. Rev. Lett.* **98**, 060404 (2007).
44. A. V. Gorshkov *et al.*, *Phys. Rev. Lett.* **101**, 073201 (2008).
45. T. Karman, J. M. Hutson, *Phys. Rev. Lett.* **121**, 163401 (2018).
46. T. Karman, *Phys. Rev. A* **101**, 042702 (2020).
47. L. Lassablière, G. Quéméner, *Phys. Rev. Lett.* **121**, 163402 (2018).
48. T. Xie *et al.*, *Phys. Rev. Lett.* **125**, 153202 (2020).
49. Z. Z. Yan *et al.*, *Phys. Rev. Lett.* **125**, 063401 (2020).
50. X. Ye *et al.*, arXiv 2010.08685 [physics.atom-ph] (17 October 2020).
51. Z. Idziaszek, G. Quéméner, J. L. Bohn, P. S. Julienne, *Phys. Rev. A* **82**, 020703(R) (2010).
52. See supplementary materials.
53. G. Günter *et al.*, *Science* **342**, 954–956 (2013).
54. S. Ravets *et al.*, *Nat. Phys.* **10**, 914–917 (2014).
55. R. Faoro *et al.*, *Nat. Commun.* **6**, 8173 (2015).
56. B. Zhu, G. Quéméner, A. M. Rey, M. J. Holland, *Phys. Rev. A* **88**, 063405 (2013).
57. G. Quéméner, M. Lepers, O. Dulieu, *Phys. Rev. A* **92**, 042706 (2015).
58. K. Matsuda *et al.*, Data for "Resonant collisional shielding of reactive molecules using electric fields." Zenodo (2020); doi:10.5281/zenodo.4156490.

ACKNOWLEDGMENTS

We thank J. L. Bohn for stimulating discussions and careful reading of the manuscript. **Funding:** Supported by NIST, ARO MURI, DARPA DRINQS, NSF QLCI OMA–2016244, and NSF Phys-1734006; G.Q. received funding from Agence Nationale de la Recherche FEW2MANY-SHIELD Project ANR-17-CE30-0015. **Author contributions:** The experimental work and data analysis were done by K.M., L.D.M., J.-R.L., W.G.T., G.V., and J.Y. Theoretical calculations were done by G.Q. All authors contributed to interpreting the results and writing the manuscript. **Competing interests:** The authors declare no competing interests. **Data and materials availability:** All data presented in this work are available through Zenodo at (*58*).

SUPPLEMENTARY MATERIALS

science.sciencemag.org/content/370/6522/1324/suppl/DC1
Materials and Methods
Fig. S1

11 September 2020; accepted 9 November 2020
10.1126/science.abe7370

Science

Resonant collisional shielding of reactive molecules using electric fields

Kyle Matsuda, Luigi De Marco, Jun-Ru Li, William G. Tobias, Giacomo Valtolina, Goulven Quéméner and Jun Ye

Science **370** (6522), 1324-1327.
DOI: 10.1126/science.abe7370

Electric field shielding of ultracold molecules

Because reactive collisions limit the lifetime of ultracold molecular ensembles, controlling chemical reactivity at ultralow temperatures has been a long-standing goal. Using large electric fields that trigger resonant dipolar interactions between potassium-rubidium molecules trapped in a quasi–two-dimensional geometry, Matsuda *et al.* report suppression of the reactive loss rate in the vicinity of the dipolar-mediated resonances by up to an order of magnitude below the background value. The proposed shielding mechanism is general and is expected to be effective in three-dimensional geometry. It could also be used for creating long-lived quantum molecular gases of other polar molecules under strong electric fields.

Science, this issue p. 1324

Science (print ISSN 0036-8075; online ISSN 1095-9203) is published by the American Association for the Advancement of Science, 1200 New York Avenue NW, Washington, DC 20005. The title *Science* is a registered trademark of AAAS.